EUROPEAN JOURNAL OF PURE AND APPLIED MATHEMATICS
2025, Vol. 18, Issue 1, Article Number 5595
ISSN 1307-5543 – ejpam.com
Published by New York Business Global

Electrohydrodynamic Stability of Walters B′ Viscoelastic Dielectric Liquid Jet Streaming With Variable Velocity Into Another Viscoelastic Fluid via Porous Medium

Mohamed F. El-Sayed[2], Doaa M. Mostafa[1,2*], Ashwaq M. F. Alrashdi[1]

[1] *Department of Mathematics, College of Science, Qassim University, Buraidah 51452, Saudi Arabia*
[2] *Department of Mathematics, Faculty of Education, Ain Shams University, Heliopolis, Roxy, Cairo, Egypt*

Abstract. A linear axisymmetric instability analysis of a streaming Walters B′ viscoelastic liquid jet with a parabolic velocity profile surrounded by viscoelastic fluid under the impact of an axial electric field via porous media is investigated in the Rayleigh and atomization modes. Only temporal instability is considered because, due to the large Weber number, both temporal and spatial instability give almost the same outcomes in the atomization regime.The dispersion relation is calculated to evaluate the growth rate of disturbances. The findings of stability analysis show that the viscoelastic parameters, electric field, velocity profile parameter, and porosity of the porous medium hinder instability for both Rayleigh and atomization modes, while the density ratio, dielectric constants, and kinematic viscosities enhance instability in both modes. Weber number hinders instability in Rayleigh mode, but it enhances instability in atomization mode. The effects of all parameters in atomization mode are found to be more unstable than those in Rayleigh mode. It is also demonstrated that the Walters B′ viscoelastic liquid jet is more stable than an inviscid liquid jet, and the breakup process in the atomization mode of instability occurs faster than in Rayleigh mode since liquid jet instability is closely related to drop formation and breakup.

2020 Mathematics Subject Classifications: 76A05, 76A10, 76E17

Key Words and Phrases: Linear stability, Porous Medium, Viscoelastic liquid jet, Electrohydrodynamics

Nomenclature

P	Liquid pressures
ρ	Liquid density
k	Wave number

*Corresponding author.
DOI: https://doi.org/10.29020/nybg.ejpam.v18i1.5595

Email addresses: mohamedfahme@edu.asu.edu.eg (M. F. El-Sayed), do.elsayed@qu.edu.sa, doaa_mohamady@edu.asu.edu.eg (D.M.Mostafa), 441212388@qu.edu.sa (A. M. F. Alrashdi)

ϵ Dielectric constant
We Weber number
φ Electric potential function
ψ Velocity potential function
σ Surface tension coefficient
λ Viscoelasticity parameter
a Cylindrical nozzle radius
k_1 Medium permeability.
ν Kinematic viscosities
ν' Kinematic viscoelasticities
I_1 Modified first-order Bessel functions of the first kind
K_1 Modified first-order Bessel functions of the second kind
I_0 Modifed zero-order Bessel functions of the first kind
K_0 Modifed zero-order Bessel functions of the second kind

1. Introduction

The problems of liquid jet instability have attracted the interest of researchers for a long time since they have applications in numerous industrial processes and machines. The breakup of liquid jets into drops is a natural phenomenon. It is used in a wide range of applications, including lubrication, oil burners, and gas turbine engines. Since non-Newtonian liquids may be involved in many of these processes, it is interesting and crucial to comprehend the mechanics underlying their instability [22, 25].

Ibrahim [18] analyzed the instability of a liquid sheet with a parabolic velocity profile and concluded that a liquid sheet with a uniform velocity is less unstable than one with a parabolic velocity. A dispersion relation that characterizes the instability of an inviscid liquid jet emanated into an inviscid gas was established by Ibrahim and Marshall [19]. According to their findings, the instability gets stronger as the jet's velocity profile gets closer to homogeneity. Moreover, instability is encouraged by rising Weber numbers and gas/liquid density ratios.

Since a wide variety of industrial applications employ non-Newtonian jets, including roll coating, paint leveling, fertilizers, and inkjet printing, it is imperative to understand their behavior. The liquid's viscoelasticity affects significantly the instability characteristic of liquid jets [10]. Many studies have examined the instability of liquid jets that are viscoelastic without an electric field [1, 4, 33, 38]. Paralleling the classical evolution of the Newtonian liquid, Middleman [29] assessed the characteristic equation that establishes the growth rate of a disturbance on a viscoelastic jet. Under the same dynamic conditions, according to the theory, depending on the viscoelastic model under study, the stability of a viscoelastic jet will be lower than that of a Newtonian jet. In an inviscid gaseous medium, non-Newtonian liquid jets were studied by Brenn et al [3]. They calculated the relevant dispersion relation between the wave number and growth rate for axisymmetric perturbations. Their study's linear stability analysis revealed that, due to the viscoelastic fluid jet's quicker growth rate of axisymmetric disturbances, a viscoelastic fluid jet with

the same Ohnesorge number is more unstable than a Newtonian fluid jet. Liu and Liu [26] investigated the stability analysis of a viscoelastic fluid jet with axisymmetric and asymmetric perturbations. They found that, for lower Weber numbers, the axisymmetric disturbance dominates over the instability of the viscoelastic liquid jet. Carroll and Joo [5] investigated the electrified viscoelastic jets, and they took into account the impact of electric field and viscoelasticity on the basic jet profile. Elasticity keeps a jet from disintegrating into droplets when it is being electrospun, according to studies by Yu et al. [40]. The importance of non-Newtonian viscoelastic fluids in industry is growing. Differential types, such as the Walters B′ type, are among these fluids; they represent the combined impact of numerous blood characteristics, including hematocrit, aggregation, plasma viscosity, and red blood cell deformability. Walters B′ fluids are essential in a wide range of industrial uses. Examples include the application of coating layers onto hard substrates, the creation of adhesive tapes, and the extrusion of plastic sheets.

The porous medium is crucial to several geophysical engineering fields, such as soil mechanics, biomechanics, petroleum industry, chemical engineering, and material science [17]. Over the past few decades, flow through porous mediums has received much attention. Numerous engineering applications across a wide range of specializations, including groundwater pollution and filtration processes, petroleum reservoirs, chemical catalytic reactors, coal combustors, ceramic processes, geophysical thermal and insulation engineering, and so on, were the driving forces behind this interest [16, 34]. The viscous term in the equation of motion of the Walters B′ viscoelastic fluid via porous material is replaced by the resistive term $-(\rho/k_1)\left[\nu - \nu`(\partial/\partial t)\right] v$, where v represents the fluid's Darcian filter velocity [36].

The study of electrohydrodynamics (EHD) is concerned with how electric fields interact with free or polarized charges in fluids, which can be strongly conducting, marginally conducting, or even excellent insulators. Therefore, EHD is the study of the interaction between fluid mechanics and an electric field. Melcher [27], Dasgupta et al. [8], Koulova and Atten [21], Del Rio and Whitaker [35], and Bendel et al. [2] have published monographs that provide a comprehensive overview of the topic of EHD and EHD through porous media. However, up until now, very little is known regarding the process of instability in electrified viscoelastic jets. The phenomenon of EHD instability in permeable media has applications in many different domains, including oil reservoir modeling, the petroleum industry, biomechanics, engineering, micro-cooling systems, nanotechnology, and the construction of thermal insulation [24, 39]. El-Sayed [12] investigated the Rayleigh and atomization modes of the EHD instability analysis of an inviscid liquid jet with a parabolic velocity into a stationary gas via a porous media and found that the instability of the system is higher in the atomization mode as compared to the Rayleigh mode. Thus, this study's objective is to examine the linear instability analysis mechanism of a viscoelastic liquid jet of Walters B′ with a parabolic velocity profile surrounded by a viscoelastic fluid in the existence of an electric field in the axial direction. The instability of viscoelastic dielectric fluid with the existence of an electric field and permeable medium has been investigated by some researchers [11, 13–15, 28].

The EHD instability of Wlaters B′ viscoelastic liquid jet was investigated in this

work when it was injected with variable velocity into another viscoelastic stationary fluid through a porous medium. Since we are interested in the area directly downstream of the nozzle, where the velocity profile relaxation occurs, the disturbances are assumed to be axisymmetric. Based on the perturbation technique and interfacial boundary conditions, the dispersion relation for this system of viscoelastic fluids has been determined. The paper is structured in the following manner: The methodology of the problem and the equations of motion are presented in Section 2. For the disturbed flow in both viscoelastic fluids, we have obtained non-dimensional linearized differential equations with solutions and the boundary conditions in sections 3 and 4 using the normal modes approach. In section. 5, we derived the dimensionless dispersion relationship and recovered some limiting cases studied before. Section 6 presents the impact of every parameter on the system's stability. Lastly, section 7 presents the closing remarks derived from the acquired results.

2. Methodology of problem

Consider a viscoelastic dielectric liquid jet (of Walters B′ type) of radius a which is fired from a nozzle at an axial velocity $(0, 0, W)$ into an otherwise quiescent stationary viscoelastic dielectric fluid environment of the same type via a medium with porosity m, and medium permeability k_1. The two viscoelastic incompressible fluids are of uniform densities ρ_1 and ρ_2, dielectric constants ϵ_1 and ϵ_2, dynamic viscosities $\mu_1\,(=\rho_1\nu_1)$and $\mu_2\,(=\rho_2\nu_2)$, uniform dynamic viscoelasticities $\mu_1'\,(=\rho_1\nu_1')$ and $\mu_2'\,(=\rho_2\nu_2')$, such that subscripts 1 and 2 distinguish the two viscoelastic fluids, where subscript 2 indicates the surrounded fluid (Fluid 1 is the jet fluid). Additionally, suppose that the entire system is influenced by a constant electric field E_0 in an axial direction. The centerline of the unperturbed jet coincides with the z-axis, which is perpendicular to the r-axis.

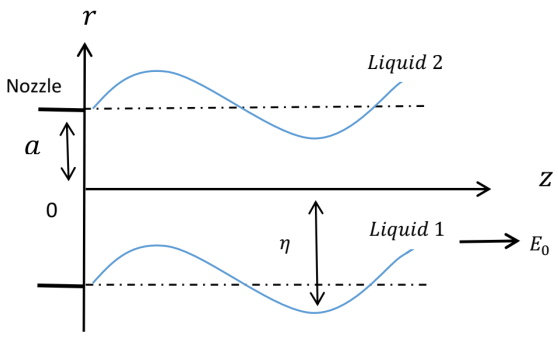

Figure 1: Physical configuration of the problem.

The basic equations of motion and continuity for the Walters B′ viscoelastic fluids via a porous media, in the two-dimensional cylindrical coordinate system (r, z) can be represented as follows [11, 16]:

$$\frac{\rho}{m}\left[\frac{\partial u}{\partial t}+\frac{1}{m}\left(u\frac{\partial u}{\partial r}+w\frac{\partial u}{\partial z}-\frac{v^2}{r}\right)\right] = -\frac{\partial P}{\partial r}-\frac{1}{k_1}\left(\mu-\mu'\frac{\partial}{\partial t}\right)u, \tag{1}$$

$$\frac{\rho}{m}\left[\frac{\partial w}{\partial t}+\frac{1}{m}\left(u\frac{\partial w}{\partial r}+w\frac{\partial w}{\partial z}\right)\right] = -\frac{\partial P}{\partial z}-\frac{1}{k_1}\left(\mu-\mu'\frac{\partial}{\partial t}\right)w, \tag{2}$$

$$\frac{\partial u}{\partial r}+\frac{u}{r}+\frac{\partial w}{\partial z} = 0. \tag{3}$$

where (u, v, w) are the components of velocity.

The dielectric constant and electric field are represented by ϵ and $\mathbf{E}$, respectively. We'll assume that the electric field $\mathbf{E}$ is non-rotational since an approximation of quasi-static behavior is valid. As a result, the electrical equations are given by [31]:

$$\nabla\cdot(\epsilon\ \mathbf{E})=0 \quad , \quad \nabla\times\mathbf{E}=0 \ \text{ and } \quad \mathbf{E}=-\nabla\varphi. \tag{4}$$

The interface between the two Walters B$'$ viscoelastic fluids is defined by $F=r-\eta$, where the following is the expression for the unit vector $\mathbf{N}$ perpendicular to the interface:

$$\mathbf{N}=\frac{\nabla F}{|\nabla F|}. \tag{5}$$

3. Perturbation equations and normal mode analysis

Due to a disturbance, let the components of electric fields, electric potentials, fluid pressures, and velocities in the perturbed state be $\left(E_0+\hat{\mathbf{E}}\right)$, $(\varphi_0+\hat{\varphi})$, $\left(P_0+\hat{P}\right)$, and $(\hat{u},\hat{v},\ (W+\hat{w}))$, then the linearizations of Eqs. (1)-(4) result in the perturbation equations shown below:

$$\frac{\rho_j}{m}\left[\frac{\partial \hat{u}_j}{\partial t}+\frac{1}{m}\left(\delta_{j1}W\frac{\partial \hat{u}_j}{\partial z}\right)\right] = -\frac{\partial \hat{P}_j}{\partial r}-\frac{\rho_j}{k_1}\left(\nu_j-\nu_j'\frac{\partial}{\partial t}\right)\hat{u}_j\ , \tag{6}$$

$$\frac{\rho_j}{m}\left[\frac{\partial \hat{w}_j}{\partial t}+\frac{1}{m}\left(\delta_{j1}\hat{u}_j\frac{\partial W}{\partial r}+\delta_{j1}W\frac{\partial \hat{w}_j}{\partial z}\right)\right] = -\frac{\partial \hat{P}_j}{\partial z}-\frac{\rho_j}{k_1}\left(\nu_j-\nu_j'\frac{\partial}{\partial t}\right)\hat{w}_j\ , \tag{7}$$

$$\frac{\partial \hat{u}_j}{\partial r}+\frac{\hat{u}_j}{r}+\frac{\partial \hat{w}_j}{\partial z} = 0, \tag{8}$$

$$\nabla\cdot(\epsilon_j\ \hat{\mathbf{E}}_\mathbf{j})=0 \quad , \quad \nabla\times\hat{\mathbf{E}}_\mathbf{j}=0 \ \text{ and } \hat{\mathbf{E}}_\mathbf{j}=-\nabla\hat{\varphi}_j\ , \quad (j=1,2)\,. \tag{9}$$

where δ_{j1} indicates Kronecker delta, for the viscoelastic fluid surrounding the viscoelastic jet, $\delta_{j1}=\delta_{21}=0$. All quantities are made dimensionless by using jet radius a and average

velocity W_{av} as follows: $\overset{*}{k} = ka$, $(\overset{*}{r}, \overset{*}{z}) = \frac{1}{a}\ (r, z)$, $(\overset{*}{u}, \overset{*}{v}, \overset{*}{w}) = \frac{1}{W_{av}}(\hat{u}, \hat{v}, \hat{w})$, $\overset{*}{E} = \frac{\hat{\mathbf{E}}}{\sqrt{\rho_1 W_{av}^2}}$, $\overset{*}{\varphi} = \frac{\hat{\varphi}}{a\sqrt{\rho_1 W_{av}^2}}$, $\overset{*}{\psi} = \frac{\hat{\psi}}{a^2 W_{av}}$, $We = \frac{\rho_1 a W_{av}^2}{\sigma}$, $\overset{*}{k}_1 = \frac{k_1}{a^2}$, $\overset{*}{\rho} = \frac{\rho_2}{\rho_1}$, $\overset{*}{p} = \frac{\hat{P}}{\rho_1 W_{av}^2}$, $\overset{*}{t} = \frac{t\, W_{av}}{a}$, $\overset{*}{\omega} = \frac{\omega a}{W_{av}}$ and $\lambda_j = \frac{\nu_j'}{a^2}$. To facilitate our analysis, the asterisks for dimensionless quantities are omitted. Hence, Eqs. (6)–(9) can be written as follows in non-dimensional forms:

$$\frac{1}{m^2}\left[m\frac{\partial u_j}{\partial t} + \delta_{j1} W \frac{\partial u_j}{\partial z}\right] = -\frac{\rho_1}{\rho_j}\frac{\partial p_j}{\partial r} - \frac{1}{k_1}\left(\nu_j - \lambda_j \frac{\partial}{\partial t}\right) u_j, \tag{10}$$

$$\frac{1}{m^2}\left[m\frac{\partial w_j}{\partial t} + \delta_{j1}\left(u_j \frac{\partial W}{\partial r} + W\frac{\partial w_j}{\partial z}\right)\right] = -\frac{\rho_1}{\rho_j}\frac{\partial p_j}{\partial z} - \frac{1}{k_1}\left(\nu_j - \lambda_j \frac{\partial}{\partial t}\right) w_j, \tag{11}$$

$$\frac{\partial u_j}{\partial r} + \frac{u_j}{r} + \frac{\partial w_j}{\partial z} = 0, \tag{12}$$

$$\nabla \cdot (\epsilon_j\ \mathbf{E_j}) = 0, \tag{13}$$

$$\nabla \times \mathbf{E_j} = 0 \quad \text{and} \quad \mathbf{E_j} = -\nabla \varphi_j\ . \tag{14}$$

The following equation is obtained by differentiating Eqs. (10) and (11) with regard to z and r, respectively, and then subtracting the second equation from the first to obtain:

$$\begin{aligned}&\left[m\frac{\partial}{\partial t} + \delta_{j1} W \frac{\partial}{\partial z} + \frac{m^2}{k_1}\left(\nu_j - \lambda_j \frac{\partial}{\partial t}\right)\right]\left(\frac{\partial u_j}{\partial z} - \frac{\partial w_j}{\partial r}\right)\\ &-\delta_{j1}\left[u_j \frac{\partial^2 W}{\partial r^2} + \frac{\partial W}{\partial r}\left(\frac{\partial u_j}{\partial r} + \frac{\partial w_j}{\partial z}\right)\right] = 0.\end{aligned} \tag{15}$$

Equations (13) and (14) can be represented in the form $\nabla^2 \varphi_j = 0$, or in the following equivalent form:

$$r\frac{\partial^2 \varphi_j}{\partial r^2} + \frac{\partial \varphi_j}{\partial r} + r\frac{\partial^2 \varphi_j}{\partial z^2} = 0. \tag{16}$$

The non-dimensional disturbance stream function ψ_j is represented as [9]:

$$u_j = \frac{1}{r}\frac{\partial \psi_j}{\partial z}, \qquad w_j = -\frac{1}{r}\frac{\partial \psi_j}{\partial r}. \tag{17}$$

which satisfies Eq. (12) identically. We use the normal mode method by seeking solutions as follows [7]:

$$[\psi_j, \varphi_j\ , p_j] = [\Psi_j(r), \Phi_j(r), P_j(r)] \exp(ikz + \omega t)\,. \tag{18}$$

By inserting Eq. (18) into Eq. (17), we get:

$$\left(u_j,\ w_j\right) = \frac{1}{r}\left(ik\Psi_j(r), -\frac{d\Psi_j(r)}{dr}\right) \exp(ikz + \omega t)\,. \tag{19}$$

Now, substituting Eq. (19) into Eq. (15), we get:

$$\begin{aligned}&\left[(m\omega + ik\delta_{j1}W) + \frac{m^2}{k_1}(\nu_j - \lambda_j\omega)\right]\left(r\frac{d^2\Psi_j}{dr^2} - \frac{d\Psi_j}{dr} - rk^2\Psi_j\right)\\ &-ik\delta_{j1}\Psi_j\left(r\frac{d^2W}{dr^2} - \frac{dW}{dr}\right) = 0.\end{aligned} \tag{20}$$

Leib and Goldstein [23] [24] represented the influence of velocity profile relaxation with a set of dimensionless parabolic velocity profiles as follows [12, 18]:

$$W(r) = \frac{1 - br^2}{1 - b/2}. \tag{21}$$

As the parameter b increases from one (Hagen-Poiseuille profile) to zero (uniform profile), it is used to create profiles that get flatter over time.

Substituting (21) into (20) and (18) into (16), we have

$$r\frac{d^2\Psi_j}{dr^2} - \frac{d\Psi_j}{dr} - rk^2\Psi_j = 0, \tag{22}$$

$$r\frac{d^2\Phi_j}{dr^2} + \frac{d\Phi_j}{dr} - rk^2\Phi_j = 0. \tag{23}$$

According to Eq. (18), the interface displacement η can be represented as follows [7]:

$$\eta = \eta_0 \exp(ikz + \omega t)\,. \tag{24}$$

where η_0 denotes the initial interface displacement.

4. Solutions and boundary conditions

The velocity along the axis of the viscoelastic liquid jet must be finite, and disturbances vanish in the surrounding viscoelastic fluid far away from the interface. Therefore, the general solutions of Eq. (22) and Eq. (23) can be represented as follows [7]:

$$\Psi_1 = \alpha_1 r I_1(kr), \qquad \Psi_2 = \alpha_2 r K_1(kr), \tag{25}$$

$$\Phi_1 = \alpha_3 I_0(kr), \qquad \Phi_2 = \alpha_4 K_0(kr). \tag{26}$$

where $\alpha_1 - \alpha_4$ are arbitrary constant.

The following linearized boundary conditions should be satisfied by the solution for Φ_j and Ψ_j, $(j = 1, 2)$:

1. The kinematic condition that each fluid particle on the interface remains on it, leads to [18]:

$$u_j = m\frac{\partial \eta}{\partial t} + \delta_{j1} W \frac{\partial \eta}{\partial z} \quad \text{at} \quad r \approx 1, \quad j = 1, 2. \tag{27}$$

2. The electric field tangential component must be continuous at the interface, which results in:

$$\left\| \frac{\partial \varphi}{\partial z} \right\| = 0, \quad \text{at} \quad r \approx 1. \tag{28}$$

where $\|\star\|$ denotes the jump across the interface.

3. Since the normal component of the electric displacement at the interface must be continuous, this results in:

$$\left\| \epsilon \frac{\partial \varphi}{\partial r} \right\| = -ik\eta E_0 \|\epsilon\|, \qquad \text{at} \quad r \approx 1. \tag{29}$$

4. The interfacial condition for momentum conservation can be expressed as [23, 26]:

$$p_1 - \epsilon_1 E_0 \frac{\partial \varphi_1}{\partial z} = p_2 - \epsilon_2 E_0 \frac{\partial \varphi_2}{\partial z} - \frac{1}{We}\left(\eta + \frac{\partial^2 \eta}{\partial z^2}\right), \quad \text{at} \quad r \approx 1, \tag{30}$$

Using Eq. (25) and substituting from Eqs. (19) and (24) into the kinematic condition (27) yields

$$\alpha_1 = -\frac{i\eta_0}{kI_1(k)}\left[m\omega + ik\left(\frac{1-b}{1-b\ /\ 2}\right)\right], \tag{31}$$

$$\alpha_2 = -\frac{im\omega\eta_0}{kK_1(k)}. \tag{32}$$

Hence, we obtain the following expressions of stream functions:

$$\psi_1 = -\frac{i\eta_0 r}{kI_1(k)}\left[m\omega + ik\left(\frac{1-b}{1-b\ /\ 2}\right)\right] I_1(kr)\exp\left(ikz+\omega t\right), \tag{33}$$

$$\psi_2 = -\frac{im\omega r\eta_0}{kK_1(k)} K_1(kr)\exp\left(ikz+\omega t\right). \tag{34}$$

Also, substituting Eqs. (18) and (26) into the conditions (28) and (29), yields after solving the resulting two equations.

$$\alpha_3 = \frac{i\eta_0 E_0\left(\epsilon_2-\epsilon_1\right)K_0(k)}{[\epsilon_1 I_1(k)K_0(k)+\epsilon_2 I_0(k)K_1(k)]}, \tag{35}$$

$$\alpha_4 = \frac{i\eta_0 E_0\left(\epsilon_2-\epsilon_1\right)I_0(k)}{[\epsilon_1 I_1(k)K_0(k)+\epsilon_2 I_0(k)K_1(k)]}. \tag{36}$$

Hence, we obtain the following expressions of electric potential functions:

$$\varphi_1 = \frac{i\eta_0 E_0\left(\epsilon_2-\epsilon_1\right)K_0(k)I_0(kr)}{[\epsilon_1 I_1(k)K_0(k)+\epsilon_2 I_0(k)K_1(k)]}\exp\left(ikz+\omega t\right) \tag{37}$$

$$\varphi_2 = \frac{i\eta_0 E_0\left(\epsilon_2-\epsilon_1\right)I_0(k)K_0(kr)}{[\epsilon_1 I_1(k)K_0(k)+\epsilon_2 I_0(k)K_1(k)]}\exp\left(ikz+\omega t\right) \tag{38}$$

The liquid pressures p_1 and p_2 may be obtained by substitution from Eqs. (18), (19), (21), (33) and (34) into Eq. (11) as follows:

$$\begin{aligned} p_1 = & -\frac{\eta_0}{m^2 kI_1(k)}\left[m\omega + ik\left(\frac{1-b}{1-(b\ /\ 2)}\right)\right] \\ & \times\left\{\left[m\omega + ik\left(\frac{1-br^2}{1-(b/2)}\right)+\frac{m^2}{k_1}\left(\nu_1-\omega\lambda_1\right)\right]I_0(kr)\right. \\ & \left.+\left(\frac{2ibr}{1-(b/2)}\right)I_1(kr)\right\}\exp\left(ikz+\omega t\right), \end{aligned} \tag{39}$$

$$p_2 = \frac{\omega\eta_0\rho}{kK_1(k)}\left[\omega+\frac{m}{k_1}\left(\nu_2-\omega\lambda_2\right)\right]K_0(kr)\exp\left(ikz+\omega t\right). \tag{40}$$

Note that, in the derivation of the above solutions, we have used the following recurrence relations [37].

$$\begin{aligned} I_0'(kr) &= kI_1(kr), & K_0'(kr) &= -kK_1(kr), \\ rI_1'(kr) &= krI_0(kr)-I_1(kr), & rK_1'(kr) &= -krK_0(kr)-K_1(kr). \end{aligned}$$

5. Derivation of the dispersion relation

The dispersion relation is obtained by substituting from Eqs. (37)–(40) and (24) into Eq. (30).

$$\begin{aligned}
&\frac{1}{m^2}\left[m\Omega + ik\sqrt{We}\left(\frac{1-b}{1-(b/2)}\right)\right]^2 \frac{I_0(k)}{I_1(k)} \\
&+\rho\left[\Omega^2 + \frac{m}{k_1}\Omega\sqrt{We}\left(\nu_2 - \frac{\Omega}{\sqrt{We}}\lambda_2\right)\right]\frac{K_0(k)}{K_1(k)} \\
&+\sqrt{We}\left[m\Omega + ik\sqrt{We}\left(\frac{1-b}{1-(b/2)}\right)\right] \\
&\times\left[\frac{1}{m^2}\left(\frac{2ib}{1-b/2}\right) + \frac{1}{k_1}\left(\nu_1 - \frac{\Omega}{\sqrt{We}}\lambda_1\right)\frac{I_0(k)}{I_1(k)}\right] \\
&+\frac{k^2E_0^2\left(\epsilon_2-\epsilon_1\right)^2 K_0(k)I_0(k)\left(We\right)}{\left[\epsilon_1 I_1(k)K_0(k) + \epsilon_2 I_0(k)K_1(k)\right]} - k\left(1-k^2\right) = 0,
\end{aligned} \tag{41}$$

where $\Omega = \omega\sqrt{We}$ is the complex non-dimension growth rate, i.e., $\Omega = \Omega_r + i\Omega_i$. From the dispersion relation (41), we conclude the following limiting cases:

(1) El-Sayed [12] has previously acquired the same dispersion relation when the viscoelastic parameters $\lambda_1 = 0$ and $\lambda_2 = 0$.

(2) We get to the same dispersion relation that Marshall and Ibrahim [19] had previously discovered in the absence of the viscoelastic term, the electric field, and the permeable medium (i.e., when $m = 1$ and $k_1 \to \infty$).

Rewriting Eq. (41) as simply as possible:

$$B_1\Omega^2 + B_2\Omega + B_3 = 0, \tag{42}$$

where

$$B_1 = \left(1 - \frac{m\lambda_1}{k_1}\right)\frac{I_0(k)}{I_1(k)} + \rho\left(1 - \frac{m\lambda_2}{k_1}\right)\frac{K_0(k)}{K_1(k)}, \tag{43}$$

$$\begin{aligned}
B_2 = {} & \sqrt{We}\left\{\frac{m}{k_1}\left[\nu_1\frac{I_0(k)}{I_1(k)} + \rho\nu_2\frac{K_0(k)}{K_1(k)}\right]\right. \\
& \left. + i\left[\left(\frac{1-b}{1-(b/2)}\right)\left(\frac{2k}{m} - \frac{k\ \lambda_1}{k_1}\right)\frac{I_0(k)}{I_1(k)} + \frac{1}{m}\left(\frac{2b}{1-b/2}\right)\right]\right\},
\end{aligned} \tag{44}$$

$$\begin{aligned}
B_3 = {} & (We)\left\{\left(\frac{1-b}{1-(b/2)}\right)\right. \\
& \left.\times\left[\left(-\frac{k^2\left(1-b\right)}{m^2\left(1-(b/2)\right)} + \frac{ik\nu_1}{k_1}\right)\frac{I_0(k)}{I_1(k)} - \frac{2kb}{m^2\left(1-b/2\right)}\right]\right.
\end{aligned}$$

$$-\frac{k\left(1-k^2\right)}{(We)}+\frac{k^2E_0^2\left(\epsilon_2-\epsilon_1\right)^2K_0(k)I_0(k)}{[\epsilon_1I_1(k)K_0(k)+\epsilon_2I_0(k)K_1(k)]}\Bigg\}. \tag{45}$$

The analytical solution of the second-order equation (42) with complex coefficients is:

$$\Omega=\frac{-B_2+\sqrt{B_2^2-4B_1B_3}}{2B_1}=\frac{-B_2+\sqrt{b_1+ib_2}}{2B_1}, \tag{46}$$

in which

$$\begin{aligned}
b_1 &= (We)\Bigg\{\frac{m^2}{k_1^2}\left(\nu_1\frac{I_0(k)}{I_1(k)}+\rho\nu_2\frac{K_0(k)}{K_1(k)}\right)^2\\
&-\frac{1}{(1-b/2)^2}\left((1-b)\left(\frac{2k}{m}-\frac{k\lambda_1}{k_1}\right)\frac{I_0(k)}{I_1(k)}+\frac{2b}{m}\right)^2\\
&+4\left[\left(1-\frac{m\lambda_1}{k_1}\right)\frac{I_0(k)}{I_1(k)}+\rho\left(1-\frac{m\lambda_2}{k_1}\right)\frac{K_0(k)}{K_1(k)}\right]\\
&\times\left[\frac{k\left(1-k^2\right)}{(We)}+\frac{2kb\left(1-b\right)}{m^2\left(1-b/2\right)^2}\right.\\
&\left.-\frac{k^2E_0^2\left(\epsilon_2-\epsilon_1\right)^2K_0(k)I_0(k)}{[\epsilon_1I_1(k)K_0(k)+\epsilon_2I_0(k)K_1(k)]}+\frac{k^2\left(1-b\right)^2}{m^2\left(1-b/2\right)^2}\frac{I_0(k)}{I_1(k)}\right]\Bigg\},
\end{aligned} \tag{47}$$

$$\begin{aligned}
b_2 &= \frac{(We)}{(1-b/2)}\Bigg\{\frac{2m}{k_1}\left(\nu_1\frac{I_0(k)}{I_1(k)}+\rho\nu_2\frac{K_0(k)}{K_1(k)}\right)\\
&\times\left[(1-b)\frac{I_0(k)}{I_1(k)}\left(\frac{2k}{m}-\frac{k\lambda_1}{k_1}\right)+\frac{2b}{m}\right]\\
&-\frac{4k\nu_1}{k_1}(1-b)\frac{I_0(k)}{I_1(k)}\left[\left(1-\frac{m\lambda_1}{k_1}\right)\frac{I_0(k)}{I_1(k)}+\rho\left(1-\frac{m\lambda_2}{k_1}\right)\frac{K_0(k)}{K_1(k)}\right]\Bigg\}.
\end{aligned} \tag{48}$$

Hence, the growth rate's real component is written as [6, 32]:

$$\begin{aligned}
\Omega_r &= \frac{1}{2}\left[\left(1-\frac{m\lambda_1}{k_1}\right)\frac{I_0(k)}{I_1(k)}+\rho\left(1-\frac{m\lambda_2}{k_1}\right)\frac{K_0(k)}{K_1(k)}\right]^{-1}\Bigg\{\sqrt{\frac{b_1+\sqrt{b_1^2+b_2^2}}{2}}\\
&-\frac{m\sqrt{We}}{k_1}\left(\nu_1\frac{I_0(k)}{I_1(k)}+\rho\nu_2\frac{K_0(k)}{K_1(k)}\right)\Bigg\}.
\end{aligned} \tag{49}$$

6. Stability discussion

Only temporal instability is taken into account here because, in the atomization regime, the Weber number is large, meaning that both temporal and spatial instability produce roughly the same results [12]. It's also interesting to compare the results obtained in this regime with those obtained in the corresponding Rayleigh regime, where the Weber number is small, as shown in the following figures.To investigate the impact of every parameter on the system's stability, use Mathematica Software (version 12.1) to plot the growth rate variation Ω_r with wave number k. A viscoelastic jet is stable if $\Omega_r < 0$, unstable if $\Omega_r > 0$, and neutrally stable if $\Omega_r = 0$, according to the temporal stability analysis that is considered here. We will be examining the growth of instabilities that occur in the Rayleigh and atomization modes. In the instability mode of the Rayleigh regime, the waves are relatively long, and $\rho We < 1$. Conversely, in the instability mode of the atomization regime, at the interface, the waves are shorter, and $\rho We > 1$. The dominant wave number is the wave number that reflects the highest growth rate. The following values of the parameters have been taken into consideration when drawing the curves of the figures: $b = 0.7$, $m = 0.3$, $k_1 = 2$, $\nu^{(1)} = 0.5$, $\nu^{(2)} = 0.3$, $\lambda_1 = 0.02$, $\lambda_2 = 0.002$, $\epsilon_1 = 0.4$, $\epsilon_2 = 0.2$, $\rho = 0.02$, $E_0 = 0.4$, $We = 10000$ (in the atomization mode), and $We = 10$ (in the Rayleigh mode).

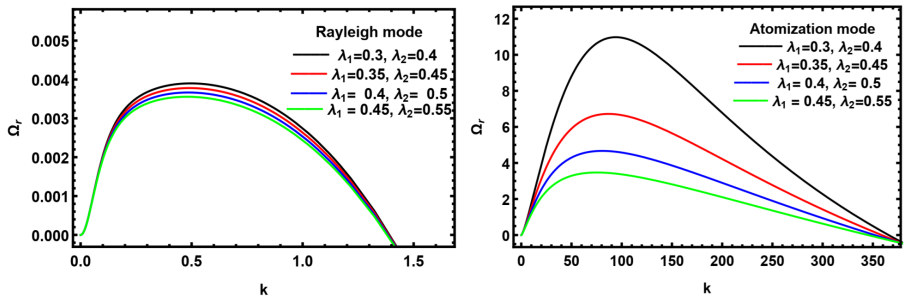

(a) (b)

Figure 2: Displays the impact of viscoelastic parameters λ_1 and λ_2 in Rayleigh and atomization modes..

Figures 2(a) and 2(b) illustrate the impact of viscoelastic parameters λ_1 and λ_2 on the instability characteristics in the Rayleigh mode and atomization mode, respectively. We have plotted the variation of the growth rate Ω_r given by Eq. (49) against k. From Fig. 2(a), in the Rayleigh mode, we can observe that in the range of wave number $0 < k < 0.1$, for all values of the viscoelastic parameters, the growth rates are the same, after which as the values of the viscoelastic parameters increase, the growth rates somewhat decline; consequently, by raising the viscoelastic parameters, the stability area slightly increases. Consequently, we get the conclusion that the viscoelastic parameters have a slightly stabilizing influence on the Rayleigh mode. As the values of the viscoelastic parameters increase, Figure 2(b) demonstrates that the maximum growth rates decrease and occur at the same dominant wave number, hence the stability zone increases. It can be concluded that the viscoelastic parameters have a stabilizing influence in the atomization

mode.The viscoelasticity is resisted by the disturbed flow, which leads to the system moving toward stability; hence, the viscoelastic parameter enhances stability. Similar results have already been obtained [1, 30, 38]. Note that the starting and end wave number points coincide in each of Rayleigh and Taylor modes, respectively such that the instability regions under the curves in atomization mode are bigger than the corresponding regions in Rayleigh mode.

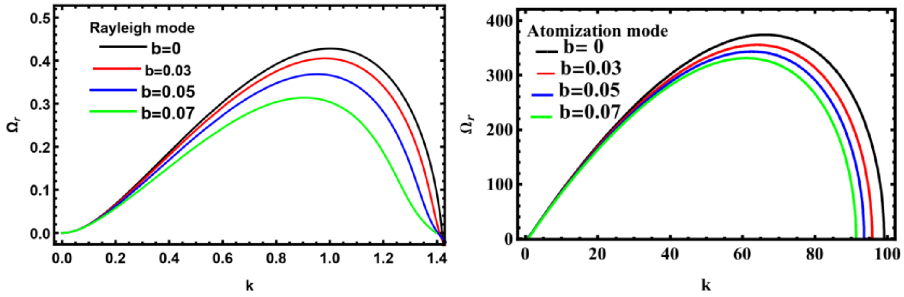

(a) (b)

Figure 3: Demonstrates the effect of velocity profile parameter b..

In Figs. 3(a) and 3(b), we have plotted the variation of the growth rate Ω_r given by Eq. (49) against k for several values of the parameter $b\,(= 0.0, 0.03, 0.05, 0.07)$ in the Rayleigh mode and atomization mode . Figures 3(a) and 3(b) demonstrate that the instability regions in the atomization mode, as well as growth rates and wave numbers period are more larger than in the Rayleigh mode. The starting and end wave number values in Rayleigh mode are, respectively, conincide, while in atomization mode the starting wave numbers of curves conincide but the ending wave numbers decrease by increasing the parameter b. When parameter b rises, the growth rate decreases, increasing the stability area. Figures 3(a) and 3(b) demonstrate that a greater value of parameter b enhances stability for both the Rayleigh and atomization modes. Similar results have already been obtained [10, 12] .

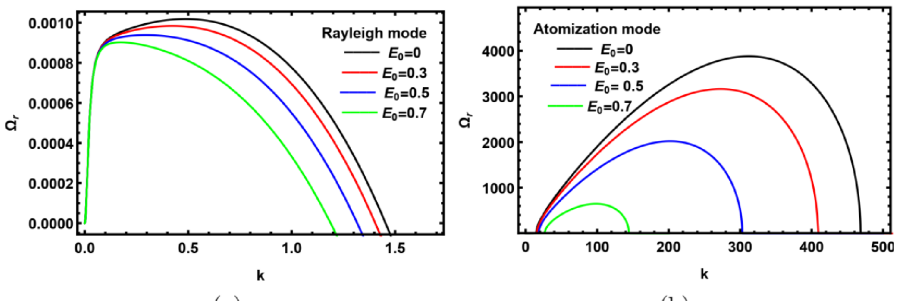

(a) (b)

Figure 4: Illustrates the impact of the electric field parameter E_0 on the stability profile..

The influence of the electric field parameter E_0 on the stability of the model under examination is represented in Figs. 4(a) and 4(b), in the Rayleigh mode and atomization mode, respectively. It can be observed from Fig. 4(a) that within the range of wave numbers $0 \leq k \leq 0.1$, the growth rates are equal. After that, stability is promoted by an increase in the electric field E_0. As the electric field parameter E_0 increases in the atomization mode, the zone of instability decreases due to a decrease in the dominant wave number and maximum growth rate, as illustrated in Fig. 4(b). We conclude that, the electric field parameter E_0 hinders the instability for both Rayleigh and atomization modes, which conforms to the results of El-Sayed [11].

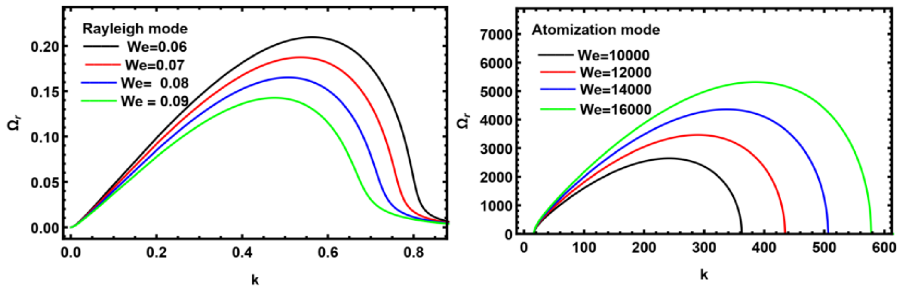

(a) (b)

Figure 5: Displays the effect of Weber number We..

Figures 5(a) and 5(b) illustrate the Weber number We influence on the disturbance growth rate, in the Rayleigh mode and atomization mode, respectively. The stabilizing effect of the We in the Rayleigh mode is demonstrated by Fig. 5(a), which makes it evident that the growth rate decreases as the We increase, and hence the stability zone is enlarged, this shows the stabilizing influence of the We in the Rayleigh mode. Fig. 5(b) shows that the dominant wave numbers and maximum growth rates rise with the Weber number in the atomization mode. Thus, we deduce that, in atomization mode, We has a destabilizing effect on the viscoelastic jet. A previous study yielded comparable outcomes [14, 19]. The ratio of surface tension to inertial forces is represented by the Weber number, hence surface tension has a destabilizing influence in the Rayleigh mode while it has a stabilizing influence in the atomization mode.

Figures 6(a) and 6(b) display the effect of the density ratio ρ on stability behavior in the Rayleigh mode and atomization mode, respectively, Figures 6(a) and 6(b) demonstrate that ρ has a destabilizing impact in the Rayleigh and atomization modes because increasing ρ enhances instability. This outcome aligns with earlier findings by Yang et al.[39]. The density ratio is directly dependent on the density of surrounding fluid and inversely on the density of the jet fluid. Hence, the density of surrounding fluid has a destabilizing nature in the system under study. From Figs. (4) and (6), it is evident that the effect of density ratio has an opposite behavior to the impact of the electric field on our system's stability in both Rayleigh and atomization modes.

Figs. 7(a) and 7(b) display how the growth rate Ω_r , as calculated by Eq. (48), varies with k for varied values of the porosity of the porous medium m in the Rayleigh

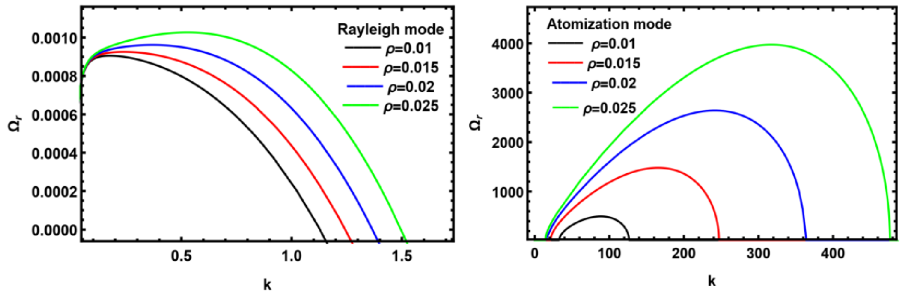

(a) (b)

Figure 6: Depicts how the stability profile is affected by the density ratio..

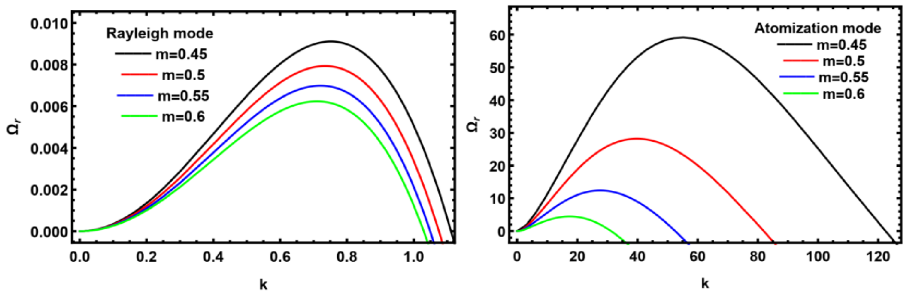

(a) (b)

Figure 7: Indicates the effect of porosity m..

and atomization modes, respectively. It is clear that, in Rayleigh mode, the maximum growth rates decrease by increasing m, thus instability area decrease. In the atomization mode, Fig. 7(b) shows that as m increases, the dominant wave number and maximum growth rates decrease. Consequently, for both Rayleigh and atomization modes, m has a stabilizing effect on the viscoelastic liquid jet in accordance with the previous study [12] of the outer gas medium and the absence of viscoelasticity parameters.

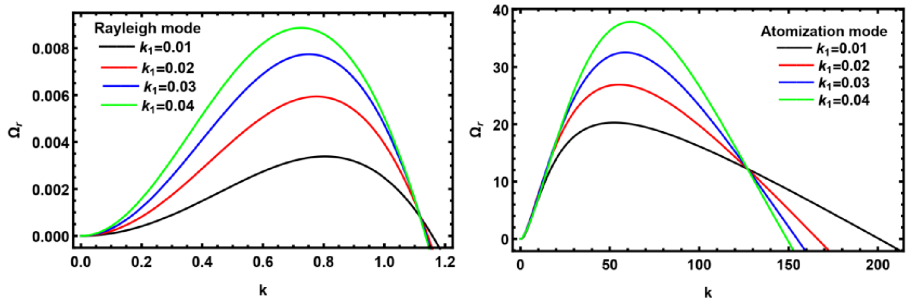

(a) (b)

Figure 8: Depicts the impact of medium permeability k_1..

In Figs. 8(a) and 8(b), the impact of the medium permeability k_1 is examined in the Rayleigh and atomization regimes, respectively. As seen in Fig. 8(a), k_1 has a destabilizing

effect in the wave number range $0 \leq k \leq 1.1$, and then a slightly stabilizing effect after that. Fig. 8(b) shows that k_1 has a destabilizing impact in the wave number range $0 \leq k \leq 127$, while it later has a stabilizing effect. Thus, we deduce that k_1 has a dual role in the stability of a viscoelastic jet in both modes, i.e., it has a destabilizing influence and then stabilizes.

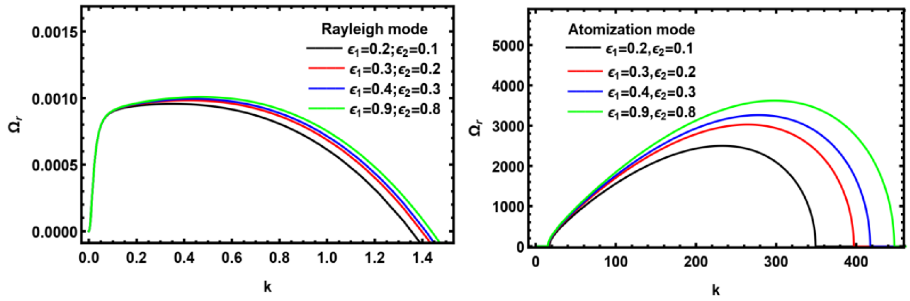

(a) (b)

Figure 9: Represents the impact of dielectric constants ϵ_1 and ϵ_2.

Figs. 9(a) and 9(b) show how the growth rate Ω_r varies with k in the Rayleigh and atomization modes, respectively, for varied values of the dielectric constants ($\epsilon_1, \epsilon_2 = 0.2, ; 0.3$, 0.2; 0.4, 0.3; 0.9, 0.8). Fig. 9(a) illustrates that, in the Rayleigh regime, growth rates are identical in value in the interval $0 \leq k \leq 0.1$; after that, a small rise in growth rates is observed through an increase in ϵ_1 and ϵ_2. Hence, ϵ_1 and ϵ_2 have a slightly destabilizing influence on the viscoelastic jet. Figure 9(b) illustrates, in the atomization regime that the instability areas increase by increasing ϵ_1 and ϵ_2. Thus, we deduce that ϵ_1 and ϵ_2 have destabilizing effects on a viscoelastic jet. It is clear from Figs. (6) and (9) that the impact of dielectric constants has quite similar behavior to the impact of ρ on the stability of our system in both Rayleigh and atomization modes.

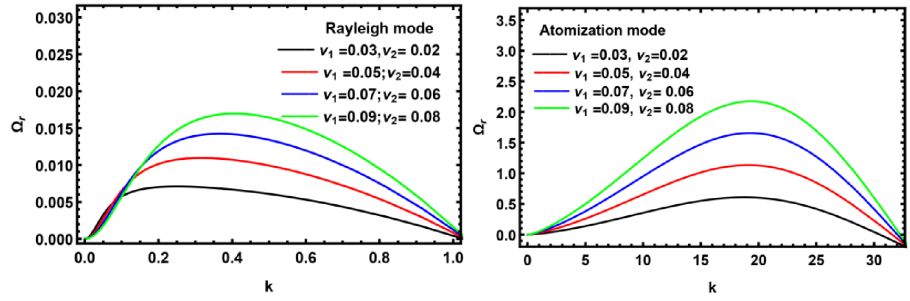

(a) (b)

Figure 10: Represents the impact of kinematic viscosities..

Figs. 10(a) and 10(b) show the behavior of the growth rate curves with respect to the kinematic viscosities in the Rayleigh and atomization modes, respectively. As can be seen from Figure 10(a), the kinematic viscosities in the Rayleigh mode have a slightly stabilizing influence in the interval $o \leq k \leq 0.09$, while they have a destabilizing influence

after that. Figure 10(b) shows that, in the atomization mode, as the kinematic viscosities increase, growth rate curves increase and the system gets destabilized. Hence, we can say that the kinematic viscosities have destabilizing effects for both instability modes except for a very small wave number range in Rayleigh mode.

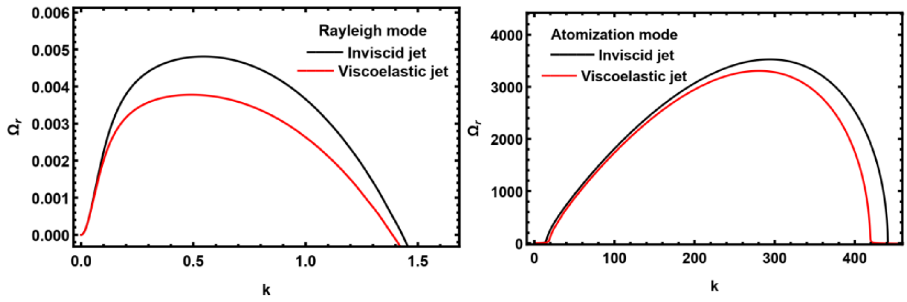

(a) (b)

Figure 11: Compare the growth rate curves of the viscoelastic jet and the inviscid liquid jet..

Figures 11(a) and 11(b) compare the growth rate curves of the Walters B′ type viscoelastic jet and the inviscid liquid jet in both Rayleigh and atomization modes, respectively. It is clear that a Walters B′ viscoelastic liquid jet has a smaller growth rate than an inviscid liquid jet. This concludes that the Walters B′ viscoelastic jet possesses greater stability than the inviscid liquid jet in both Rayleigh and atomization modes. Awasthia et al. [1] have already achieved comparable outcomes.

7. Conclusions

The temporal linear instability behavior of a streaming Wlaters B′ viscoelastic liquid jet with a parabolic velocity profile surrounded by a viscoelastic fluid of the same type with the existence of an axial electric field and porous medium in both Rayleigh and atomization modes has been examined in this study. Only temporal instability is considered because, due to the large Weber number, both temporal and spatial instability give almost the same outcomes in the atomization regime [20]. A dispersion relation has been derived. The influence of various physical parameters such as viscoelastic parameters, electric field parameters, density ratio, porosity and permeability of the porous medium, dielectric constants, and the Weber number have been illustrated through various figures. The important outcomes that were achieved are that the viscoelasticity of Walters B′ liquid jet inhibits the growth of instability, the viscoelastic parameters have a stabilizing influence for both Rayleigh and atomization modes, the velocity profile parameter has a stabilizing influence in both modes, the electric field parameter hinders instability in both modes, in the Rayleigh mode, the Weber number hinders instability, while in the atomization mode it enhances instability, the higher density of the jet fluid promotes stabilization in both regimes, the medium's permeability plays two roles in the system's stability, in both modes, the porous medium's porosity has a stabilizing nature, the dielectric constants have a slightly destabilizing nature in Rayleigh mode, while they have a destabilizing

influence in the atomization mode, kinematic viscosity plays dual roles in the system's stability in Rayleigh mode, having a stabilizing and then destabilizing effect while having a destabilizing effect in atomization mode, viscoelastic jets are more stable than inviscid jets in the Rayleigh and atomization modes and breakup phenomena in the atomization mode of instability occur faster than in the Rayleigh mode, due to the liquid jet instability behavior.

Data availability

All data that support the findings of this study are included within the article.

References

[1] M. K. Awasthia, R. Asthanab, and G. S. Agrawal. Viscoelastic potential flow analysis of the stability of a cylindrical jet. *Scientia Iranica*, 21:578–586, 2014.

[2] P. Bendel, M. Bernardo, and J. H. Dunsmui. Thomann H. Electric field driven flow in natural porous media. *Magn. Reson. Imaging*, 21:321–327, 2003.

[3] G. Brenn, Z. Liu, and F. Durst. Linear analysis of the temporal instability od axisymmetrical non-Newtonian liquid jets. *Int. J. Multiphase Flow*, 26:1621–1644, 2000.

[4] P. O. Brunn and E. Ryssel. The linear stability of a viscoelastic jet (liquid cylinder) surrounded by another viscoelastic fluid. *Z. Angew. Math. Mech.*, 83:622–628, 2003.

[5] C. P. Carroll and Y. L. Joo. Electrospinning of viscoelastic Boger fluids: Modeling and experiments. *Phys. Fluids*, 6:53–65, 2006.

[6] S. Chandrasekhar. *Hydrodynamic and Hydromagnetic Stability.* Dover Publications, New York, 1981.

[7] F. Charru. *Hydrodynamic Instabilities.* Cambridge University Press, New York, 2011.

[8] D. Dasgupta, S. Nath, and D. Bhanja. A study on dual role of viscosity on the stability of a viscous planar liquid sheet surrounded by inviscid gas streams of equal velocities, and prediction of resulting droplet distribution using maximum entropy formulation. *Phys. Fluids*, 31:22, 2019.

[9] P. G. Drazin and W. H. Reid. *Hydrodynamic Stabilities.* Cambridge University Press, New York, 1981.

[10] R. Z. Duan, Z. Y. Wang, Z. Y. Chen, and L. S. Liu. Two-dimensional temporal instability of a viscoelastic liquid sheet of a parabolic velocity profile. *Atom. Sprays*, 27:423–438, 2017.

[11] M. F. El-Sayed. Electrohydrodynamic instability of two superposed Walters B' viscoelastic fluids in relative motion through porous medium. *Arch. Appl. Mech*, 71:717–732, 2001.

[12] M. F. El-Sayed. Electrohydrodynamic instability of atomization and Rayleigh regimes for a dielectric liquid jet emanated with parabolic velocity profile into a stationary dielectric gas through porous medium. *Special Topics Rev. Porous Medd*, 9:329–345, 2018.

[13] M. F. El-Sayed and A. M. Alanzi. Electrohydrodynamic instability of atomization and Rayleigh regimes for a dielectric liquid jet emanated with parabolic velocity profile into a stationary dielectric gas through porous medium. *Fluids*, 7:247, 2022.

[14] M. F. El-Sayed, M. F. E. Amer, and Z. S. Alfayzi. Electrohydrodynamic Couette–Poiseuille Flow Instability of Two Viscous Conducting and Dielectric Fluid Layers Streaming through Brinkman Porous Medium. *Mathematics*, 11:3281, 2023.

[15] M. F. El-Sayed, N. T. Eldabe, M. H. Haroun, and D.M. Mostafa. Nonlinear electroviscous potential flow instability of two superposed couple-stress fluids streaming through porous medium. *J. Porous Med.*, 17:405–420, 2014.

[16] M. F. El-Sayed, G. M. Moatimid, F. M. F. Elsabaa, and M. F. E. Amer. Axisymmetric and asymmetric instabilities of a non-Newtonian liquid jet moving in an inviscid gas through porous media. *J.Porous Med.*, 19:751–760, 2016.

[17] R. A. Greenkorn. *Flow Phenomena in Porous Media: Fundamentals and Applications in Petroleum, Water, and Food Production.* Marcel Dekker, New York, 2023.

[18] E. A. Ibrahim. Instability of a liquid sheet of parabolic velocity profile. *Phys. Fluids*, 10:1034–1036, 1998.

[19] E. A. Ibrahim and S. Q. Marshall. Instability of a liquid jet of parabolic velocity profile. *Chem. Eng. Sci.*, 76:17–21, 2000.

[20] J. B. Keller, S. I. Rubinow, and Y. O. Tu. Spatial instability of a jet. *Phys. Fluids*, 16:2052, 1973.

[21] D. Koulova and P. Atten. EHD instabilities of two layers of insulating and conducting immiscible liquid subjected to unipolar injection. *Fluids*, 9:200, 2024.

[22] J. C. Lasheras and E. J. Hopfinger. Liquid jet instability and atomization in a coaxial gas stream, Ann. Rev. *Fluid Mech*, 32:275–308, 2000.

[23] S. J. Leib and M. E. Goldstein. The generation of capillaty instabilities on a liquid jet. *J. Fluid Mech.h*, 168:479–500, 1986.

[24] F. Li, Xie yuan Yin, and Xiezhen Yin. Axisymmetric and non-axisymmetric instability of an electrically charged viscoelastic liquid jet. *Fuel Energy Abst*, 166:1024–1032, 2011.

[25] S. P. Lin and K. J. Ruschak. Breakup of Liquid Sheets and Jets. *Applied Mechanics Reviews*, 57, 2004.

[26] Z. Liu and Z. Liu. Instability of viscoelastic liquid jet with axisymmetic and asymmetric disturbances. *Int. J. Multiphase Flow*, 34:42–60, 2008.

[27] J. R. Melcher. *Continuum Electromechanics.* MIT Press, Cambridge, 1981.

[28] T. M. N. Metwaly and N. M. Hafez. Electroviscoelstic Stability Analysis of Cylindrical Structures in Walters B Conducting Fluids Streaming through Porous Medium. *Fluids*, 7:224, 2022.

[29] S. Middleman. Stability of a viscoelastic jet. *Chem. Eng. Sci.*, 28:1037–1040, 1965.

[30] D. M. Mostafa. Viscoelastic potential flow instability theory of Rivlin-Ericksen electrified fluids of cylindrical interface. *J. Ocean Eng. Sci.*, 9(4):311–3160, 2024.

[31] S. Ozgen and O. Uzol. Investigation of the linear stability problem of electrified jets: Inviscid analysis. *J. Fluids Eng.*, 134:091201, 2012.

[32] J. P. Pascal. Instability of power-law fluid down a porous incline. *J. Non-Newtonian Fluid Mech.*, 133:109–120, 2006.

[33] C. Patrascu and C. Balan. Temporal instability of a viscoelastic liquid thread in the presence of a surrounding viscoelastic fluid. *J. Non-Newtonian Fluid Mech.*, 261:164–

170, 2018.

[34] I. Pop and D. B. Ingham. Convective Heat Transfer: Mathematical and Computational Modeling of Viscous Fluids and Porous Media. *Pergamon, oxford*, 261:164–170, 2018.

[35] J. A. Del Rio and S. Whitaker. Electrohydrodynamics in porous media. *Trans. Porous Med*, 44:385–405, 2019.

[36] B. Straughan. *Stability and Wave Motion in Porous Media, Applied Mathematical Sciences.*, volume 165. Springer-Verlad, New York, 2008.

[37] G. N. Watson. *A Treatise on the Theory of Bessel Functions, 2nd Edition.*, volume 2nd Edition. Cambridge University, New York, 1995.

[38] L. J. Yang, M. L. Du, Q. F. Fu, and W. Zhang. Linear stability analysis of a power-law liquid jet. *Atom. Sprays*, 22:123–141, 2012.

[39] L. J. Yang, Y. X. Lin, and Q. F. Fu. Linear stability analysis of an electrified viscoelastic liquid jet. *J. Fluids, Eng.*, 134:071303, 2012.

[40] J. H. Yu, S. V. Fridrikh, and G. C. Rutledge. The role of elasticity in the formation of electrospun Fibers. *Polymer*, 47:4789–4797, 2006.